Proceedings World Geothermal Congress 2026
Calgary, Canada, June 8 – 11, 2026

Reaction Path Modelling in Basalt–CO_2–H_2O Flow-Through Experiments

Koji Mori[1]*, Atsushi Neyama[1], Kentaro Masuoka[2], Hajime Yamamoto[2], Naoki Nishiyama[3], Masao Sorai[3] and Amane Terai[4]

Blue Earth Security Co., Ltd.[1]*, Taisei Corporation[2], National Institute of Advanced Industrial Science and Technology (AIST)[3], Japan Organization for Metals and Energy Security (JOGMEC)[4]

mori@besec.co.jp

Keywords: Supercritical CO_2, Geothermal reservoir, Basalt–CO_2–H_2O system, THC, Column experiments

INTRODUCTION

In the development of CO_2 geothermal power generation, where CO_2 is injected into geothermal reservoirs for heat extraction, the geochemical interactions between supercritical CO_2 and reservoir rocks under high-temperature and high-pressure conditions are not yet fully understood. In particular, the impacts of secondary mineral precipitation and re-dissolution on reservoir porosity and permeability remain insufficiently clarified.

To elucidate these geochemical mechanisms, we conducted reactive transport modeling to reproduce flow-through column experiments involving basalt–CO_2–H_2O systems and to identify the dominant reaction pathways. The results indicate the coexistence of two or more distinct flow regimes within the basalt–CO_2–H_2O system. Among these, we focused on a flow path composed of interconnected micropores. A thermo-hydro-geochemical (THC)-coupled reaction path model was developed, which successfully reproduced the observed solute concentrations, secondary mineral precipitation, and post-experiment mass loss across three experimental cases with different pressure differentials.

The calibrated model was subsequently extended to a field-scale demonstration using a typical 5-spot well configuration. The simulation focused on the short-term behavior following CO_2 injection, providing insights into the early-stage geochemical and hydrological responses of geothermal reservoirs under CO_2-based exploitation scenarios.

1 OVERVIEW OF THE LABORATORY COLUMN FLOW-THROUGH EXPERIMENT

Flow-through column experiments for the basalt–CO_2–H_2O system were obtained from Nishiyama et al. (2024) In these experiments, CO_2-saturated water was prepared under conditions of 200 °C and 10 MPa and injected into the inlet of a cylindrical basalt core sample using a syringe pump for approximately 20 days. Three test cases—D-Bst06, D-Bst09, and D-Bst10—were conducted, each with a different applied differential pressure to control the flow rate (see Table 1). The actual flow velocities within the samples ranged from 30 to 650 cm/d.

Available experimental data includes time-series variations of elemental concentrations in the outlet solution, mineralogical compositions, and changes in effluent volume. Post-experiment solid-phase analyses revealed significant mineral dissolution and secondary mineral precipitation near the inlet surface (< 1 mm), including dissolution of Al-rich phases, amorphous silica, plagioclase, olivine, clinopyroxene, and basaltic glass. In distal regions (10–200 mm from the inlet), secondary porosity development and mineral precipitation were observed in association with CO_2 infiltration. These secondary phases included fibrous minerals, smectite-like clay phases, Fe-rich precipitates, reticulated structures, and pore-filling minerals, which collectively reduced porosity in these zones. For additional experimental details and results, refer to Nishiyama et al. (2024).

2 THC MODELING AND SIMULATION

Laboratory-scale thermo-hydro-geochemical (THC) phenomena were investigated using a one-dimensional column packed with basalt core samples, with CO_2-saturated water injected under three different pressure conditions (Table 1).

Figure 1(b) illustrates the conceptual model of the flow-through column shown in the photograph of Figure 1(a). As shown in Figure 1(c), the entire flow path of the basalt core sample was represented by ten grid blocks, with additional boundary cells attached at both ends. The initial conditions were set to a pressure of 10 MPa and a temperature of 200 °C, with the initial CO_2 saturation in the sample set to zero. The upper and lower ends of the column were assigned constant-pressure boundaries, and the inlet boundary condition was adjusted so that the overall pressure gradient along the flow path matched that of the experimental setup. The initial aqueous

composition was defined as distilled water with pH 7. Following the experimental procedure, the system was first allowed to undergo initial water–rock interaction for approximately 0.5 days under the specified temperature and pressure conditions before the injection of CO_2-saturated water. Using this short-term interacted state as the new initial condition, a 20-day flow-through simulation with CO_2-saturated water was then conducted.

The numerical simulation was performed using TOUGHREACT V4.13-OMP with the ECO2N V2.0 (Sonnenthal et al., 2021), employing the double-permeability model. A single-permeability model was first applied to simultaneously reproduce both geochemical observations (elemental concentrations at the column outlet) and hydraulic measurements (declining flow rates at the column outlet) as performance indicators. However, this approach could not adequately reproduce both measurement datasets. Furthermore, experimental observations indicated selective reactions along preferential flow paths within the column. These findings suggest that the injected CO_2 in the basalt sample migrated through two or more distinct flow paths: one representing relatively homogeneous flow through the porous medium, and the other characterized by preferential flow accompanied by reductions in porosity and permeability due to secondary mineral precipitation. Consequently, a double-permeability model as shown in Figure 1(c) was adopted to better account for these heterogeneous flow and reaction processes.

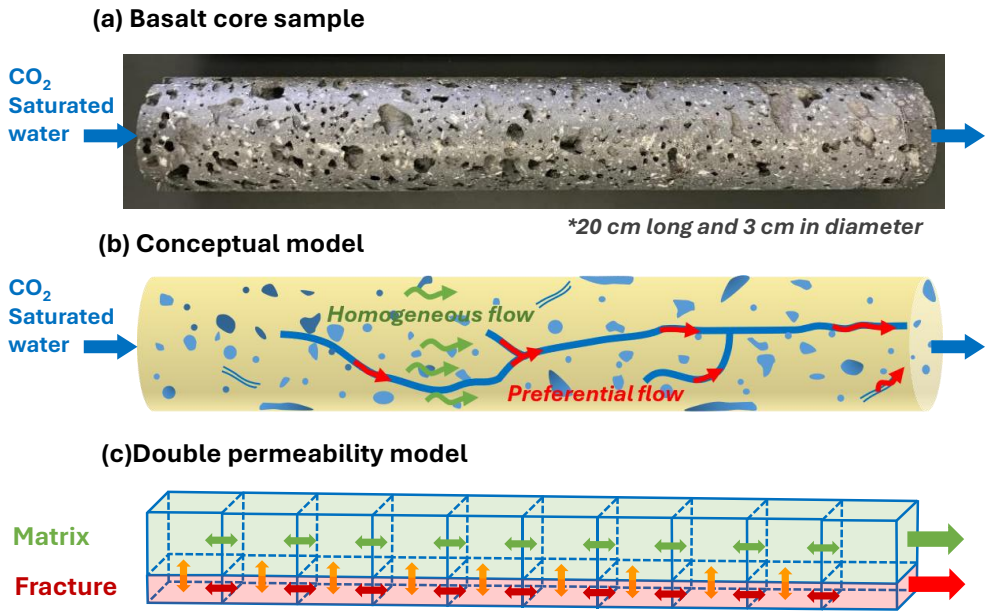


Figure 1 Conceptual and numerical models of the basalt core sample used in this study: (a) Basalt core sample, (b) conceptual model, (c) double-permeability numerical mesh.

Table 1 Basic parameters for the Thermal–Hydrological (TH) processes

Parameters		Unit	Applied value	
Core geometry (length/diameter)		m	Cylindrical column (0.2/0.03)	
Volume fraction		-	Fracture 0.1, Matrix 0.9	
Pore compressibility		Pa^{-1}	$4.5x10^{-10}$	
Thermal expansion rate		$°C^{-1}$	$1.0x10^{-5}$	
Absolute permeability		m^2	Fracture $9.1x10^{-16}$, Matrix $1.1x10^{-17}$	
Porosity		-	Fracture 0.05, Matrix 0.23	
Thermal conductivity		W m^{-1} K^{-1}	2.5	
Specific heat		J $kg^{-1}K^{-1}$	920	
Solid density		kg m^{-3}	2960	
Initial condition				
	Pressure	MPa	10	
	Temperature	°C	200	
	CO_2 fraction	-	0.0	
Boundary condition				
	D-Bst06	MPa	4.2	*(Differential pressure)*
	D-Bst09	MPa	0.6	*(Differential pressure)*
	D-Bst10	MPa	0.08	*(Differential pressure)*

The candidate secondary mineral species were first selected based on mineralogical analyses of the basalt sample. In addition, a separate preliminary simulation was performed to examine the rapid temporal variations in saturation indices (SI) observed immediately after the start of the experiment. Based on these independent analyses, the major primary and secondary mineral phases were identified and finalized from a wide range of potential mineral species. Following these iterative refinement procedures, the initial mineral assemblage of the basalt column sample was defined using representative basalt compositions, consisting of plagioclase 39.4 wt% (19.7 wt% albite and 19.7 wt% anorthite), pyroxene 17.0 wt% (8.5 wt% enstatite and 8.5 wt% diopside), olivine 2.5 wt% (1.25 wt% forsterite and 1.25 wt% fayalite), K-feldspar 19.7 wt%, and silica 14.6 wt%, including amorphous SiO_2. These primary minerals were assigned by kinetic dissolution rate laws based on Palandri and Kharaka (2004), incorporating neutral, acidic, and basic reaction mechanisms for each mineral. Similar kinetic datasets were applied to the primary minerals, allowing the model to capture the distinct dissolution behavior of highly reactive olivine and pyroxenes relative to more slowly dissolving silicate phases.

To describe the precipitation–dissolution behavior observed in the column experiments, a suite of secondary minerals—Boehmite, Calcite, Dolomite, Beidellite (Na), and H-montmorillonite—was included under equilibrium-controlled reaction conditions. Boehmite and Beidellite serve as key sinks for dissolved Al, while carbonate minerals (Calcite and Dolomite) represent major precipitates formed through reactions with CO_2-charged water. This combination of kinetic primary-mineral dissolution and equilibrium secondary-mineral reactions enabled the model to reproduce the spatial and temporal evolution of aqueous Al and Si concentrations, as well as the associated pH buffering behavior observed in the basalt–H_2O–CO_2 column experiments.

In the simulation runs, only the boundary conditions corresponding to the three independent pressurized test cases (i.e., D-Bst06, D-Bst09, and D-Bst10) listed in Table 1 were varied, whereas all other parameters related to the THC coupled-model were kept unchanged. The thermodynamic data were taken from the THERMODEM database published by the French Geological Survey (Blanc et al., 2012).

3 RESULTS AND DISCUSSION

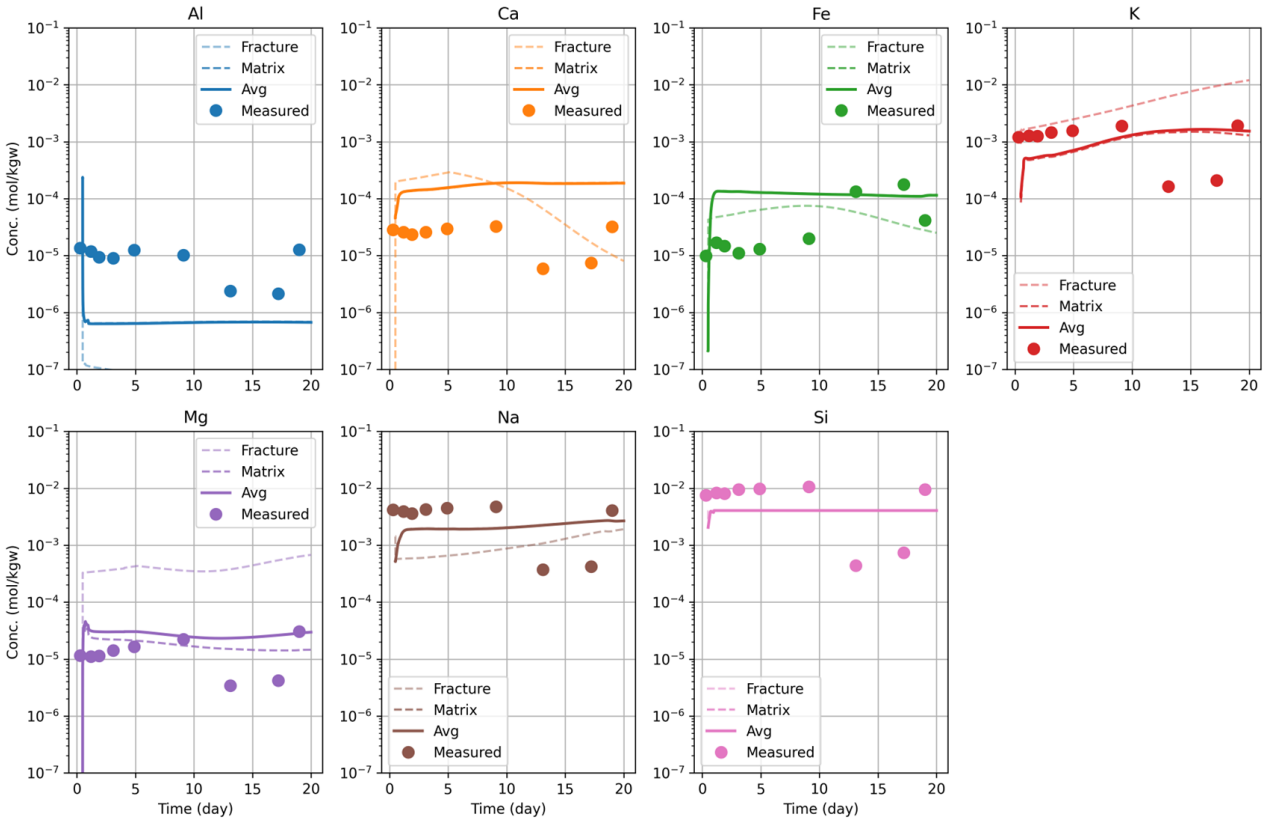
Figure 2(a) presents the simulated and measured time evolution of aqueous concentrations for major elements (Al, Ca, Fe, K, Mg, Na, and Si) at the column outlet for the experimental case D-Bst06, which was conducted under a differential pressure of 4.2 MPa. The solid lines represent the calculated average concentrations of carbonated water discharged from the fracture and matrix domains, whereas the dashed lines correspond to the individual fracture and matrix contributions. The measured data are plotted as solid circles for comparison. To reproduce the experimental results, the reactive surface areas per unit volume (S/V) of the primary minerals were iteratively calibrated until the observed concentration trends were reasonably captured. Importantly, the calibrated S/V values were not constrained by aqueous concentrations alone; they were identified as a consistent parameter set that simultaneously reproduced the measured outlet flow rates, the occurrence and distribution of secondary mineral precipitation, and the experimentally estimated permeability reduction, without internal inconsistencies among these independent observations.

The model successfully reproduced both the magnitude and temporal evolution of the measured elemental concentrations, as well as the precipitation of secondary minerals such as boehmite and smectite observed in post-experimental mineralogical analyses, thereby supporting the validity of the proposed reaction mechanisms. These results indicate that the adopted kinetic rate laws and the calibrated reactive surface areas (Figure 2(a)) appropriately represent the basalt–CO_2–H_2O system under the given thermal and hydraulic conditions. The observed aqueous concentrations of the major elements were well reproduced by the model through the dominant dissolution and precipitation reactions of representative minerals. For example, Ca and Mg concentrations were governed mainly by the dissolution of plagioclase, pyroxene, and olivine, while Al concentrations were controlled by the precipitation of clay minerals such as beidellite and montmorillonite. These representative trends were consistent with those of the other major elements, confirming that the assumed mineral reactions appropriately captured the overall geochemical behavior of the basalt–CO_2–H_2O system. These consistent tendency between the simulations and measurements confirm that the double-permeability representation, accounting for both matrix and fracture domains, successfully captures the dominant geochemical processes and mass-transfer characteristics observed in the 20-day CO_2-saturated water flow-through experiment. Furthermore, the calibrated reactive surface areas identified from the D-Bst06 simulation were applied to the other two test cases (D-Bst09 and D-Bst10) with different differential pressures, and the model also reproduced the experimental results with good agreement.

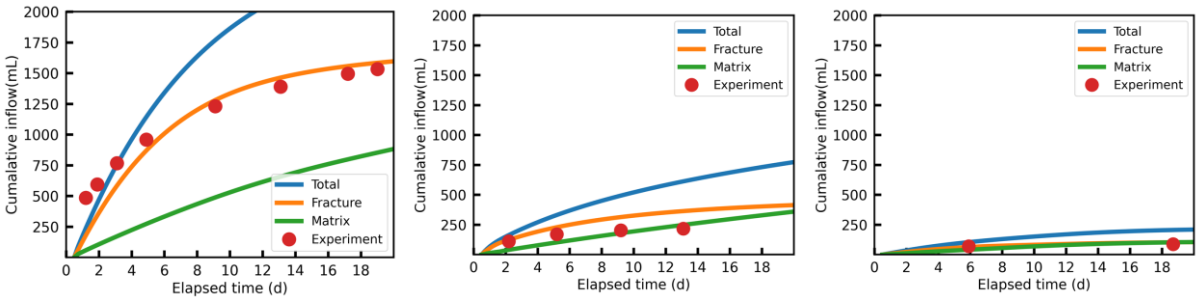
Figure 2(b) shows the cumulative flow rate at the column outlet under three loading conditions. Together, these results confirm that, although the calculated flow rate increased with higher differential pressure, the gradual

decline in flow rate over time was also captured, indicating that porosity and permeability reduction due to secondary mineral precipitation were appropriately represented in the model.

In this calibration process, the specific surface area–to–volume ratios (S/V) of the primary minerals were also identified. The resulting S/V values ranged from approximately 10^2 m^2/m^3 for slowly reacting minerals such as microcline to 10^3–10^4 m^2/m^3 for more reactive phases including olivine and pyroxenes, yielding a consistent kinetic parameter set capable of reproducing the observed outlet concentrations. These calibrated S/V values likely integrate multiple micro-scale rock–CO_2–water interaction processes—such as surface renewal, localized dissolution–precipitation cycling, and transient pore-structure modification—and therefore represent effective rather than uniquely identifiable physical parameters. Further refinement and independent validation will be necessary to better constrain the mechanistic origins of these effective S/V values.



(a)Simulated average aqueous concentrations at the outlet (solid lines) compared with measurements (dots) for D-Bst06 under a differential pressure of 4.2 MPa.



(b)Simulated cumulative outflow (solid lines) compared with measurements (dots) under differential pressures of 4.2 MPa (left), 0.6 MPa (middle), and 0.08 MPa (right).

Figure 2. Comparison between simulation (lines) and observations (dots): (a) aqueous element concentrations and (b) cumulative outflow at the column outlet.

4 PRELIMINARY FIELD-SCALE APPLICATION

To evaluate the scalability of the THC reaction-path model identified from the basalt–CO_2–H_2O column experiments, the model was applied to a two-dimensional field-scale setting. A representative numerical

experiment was performed using a five-spot well configuration with 1-km spacing between adjacent wells, under reservoir conditions of 10 MPa and 150 °C, and a total simulation period of approximately six years. Although the corresponding figure is omitted due to space limitations, several characteristic spatial trends were consistently reproduced in the field-scale simulations.

The temperature and pressure distributions remained strongly influenced by the imposed boundary conditions, whereas the geochemical fields exhibited pronounced spatial evolution driven by CO_2-charged water injection. The pH decreased markedly along the upper flow path from the injection well, accompanied by elevated concentrations of dissolved HCO_3^- resulting from enhanced CO_2–rock interactions. Dissolved Al concentrations showed a clear depletion zone forming downstream of the injection point, reflecting the progressive precipitation of secondary Al-bearing minerals.

Among the secondary phases, boehmite precipitated extensively along the advancing reaction front, whereas saponite and/or beidellite formation occurred more broadly within the altered zone. These mineral accumulation patterns were accompanied by measurable decreases in the K/K_0 ratio, indicating progressive loss of feldspar reactivity and associated porosity reduction. Collectively, these results demonstrate that the reaction pathways identified at the column scale—involving basalt dissolution, acidification, and secondary mineral formation—persist and self-organize into coherent spatial structures when extended to reservoir-relevant temporal and spatial dimensions.

5 CONCLUSIONS

This study developed a thermal–hydro–chemical (THC) reaction-path model for basalt–CO_2–H_2O systems by reproducing flow-through column experiments conducted under geothermal conditions. The TOUGHREACT simulations successfully matched both the measured elemental concentrations and the time-dependent decline in flow rate across three differential-pressure cases. Through this calibration, the specific surface area–to–volume ratios (S/V) of the primary minerals were also constrained, yielding values on the order of 10^2–10^4 m^2/m^3 depending on mineral reactivity. These S/V values likely integrate multiple micro-scale rock–CO_2–water interaction processes and therefore represent effective parameters whose mechanistic origins warrant further refinement and independent validation.

The calibrated reaction-path model was subsequently applied to a field-scale five-spot configuration. The simulation reproduced characteristic geochemical structures such as pH reduction, HCO_3^- enrichment, Al depletion, and precipitation of boehmite and saponite along the advancing reaction front, indicating that the dominant reaction pathways identified at the column scale persist under reservoir-relevant conditions.

Overall, the integrated laboratory–simulation–field approach provides a practical basis for predicting early-stage CO_2–rock interactions in basaltic geothermal reservoirs and for assessing potential geochemical impacts on reservoir performance during CO_2-based geothermal exploitation.

Acknowledgments

This study is part of the outcomes of the project “Carbon Recycling CO_2 Geothermal Power Generation Technology,” conducted under the Geothermal Power Generation Technology Research and Development Program by the Japan Organization for Metals and Energy Security (JOGMEC) in fiscal year 2021 and beyond.

REFERENCES

Eric Sonnenthal, Nicolas Spycher, Tianfu Xu, Liange Zheng (2021). TOUGHREACT V4. 13-OMP & TReactMech V1. 0. Geochemical and Reactive-Transport User Guide. Lawrence Berkeley National Laboratory.

James L. Palandri, Yousif K. Kharaka (2004). A compilation of rate parameters of water-mineral interaction kinetics for application to geochemical modeling (No. 2004-1068). US Geological Survey.

N. Nishiyama, M. Sorai, K. Masuoka, A. Terai (2024). Permeability evolution caused by CO_2-water-rock reactions under geothermal conditions: effect of rock type, Abstracts with Programs. 2024 Annual Meeting. Geothermal Research Society of Japan.

Pan, L., Spycher, N., Doughty, C., & Pruess, K. (2014). ECO2N V. 2.0: A New TOUGH2 Fluid Property Module for Mixtures of Water, NaCl, and CO_2.

Ph. Blanc, A. Lassin, P. Piantone, M. Azaroual, N. Jacquemet, A. Fabbri, E.C. Gaucher (2012): Thermoddem: A geochemical database focused on low temperature water/rock interactions and waste materials. Applied Geochemistry, 27(10). 2107~2116.